Applied Surface Science 303 (2014) 118–124

Contents lists available at ScienceDirect

Applied Surface Science

journal homepage: www.elsevier.com/locate/apsusc

Modification of Cu surface with picosecond laser pulses

J. Vincenc Oboňa[a,b], V. Ocelík[a,*], J.C. Rao[a], J.Z.P. Skolski[c], G.R.B.E. Römer[c], A.J. Huis in 't Veld[c,d], J. Th. M. De Hosson[a]

[a] Materials innovation institute M2i, Department of Applied Physics, University of Groningen, Nijenborgh 4, 9747 AG Groningen, The Netherlands
[b] Materials innovation institute M2i, Faculty of Engineering Technology, Chair of Applied Laser Technology, University of Twente, P.O. Box 217, 7500 AE, Enschede, The Netherlands
[c] Faculty of Engineering Technology, Chair of Applied Laser Technology, University of Twente, P.O. Box 217, 7500 AE, Enschede, The Netherlands
[d] TNO Technical Sciences; Mechatronics, Mechanics and Materials, De Rondom 1, 5600 HE, Eindhoven, The Netherlands

ARTICLE INFO

Article history:
Received 11 November 2013
Received in revised form 18 February 2014
Accepted 19 February 2014
Available online 28 February 2014

Keywords:
Ultra-short laser pulse
Surface modification
Incubation
Electron microscopy

ABSTRACT

High purity, mirror-polished polycrystalline Cu surface was treated with single picosecond laser pulses at fluence levels close to the single-pulse modification threshold. The induced surface topography and sub-surface changes were examined with scanning and transmission electron microscopy, respectively. The analysis showed an increased absorption of laser energy on the microscopic surface topography inhomogeneities, even at a fluence level below the modification threshold. Many features, like spikes, bubbles, spheres, as well as small periodic ripples at the bottom of scratches, reveal a significant influence of melting and eruptive relaxation of the absorbed laser energy on the final appearance of the surface. Further, it was found that thermal stresses result in twinning to a depth of few tens of nanometers under the surface. Voids at this depth have been observed as well. The results of the observations provide new insights into the early stages of the picosecond laser pulse modification of metals, especially metals with a weak electron–phonon coupling.

© 2014 Elsevier B.V. All rights reserved.

1. Introduction

In the last decade, considerable attention has been paid to the use of ultra-short laser pulses for surface modification of various metals [1–3], semiconductors [3–5], and dielectrics [3,6,7] or volume modification in transparent dielectrics [8,9]. Due to a low diffusion of the absorbed energy at moderate fluence, the technique offers a lateral structuring accuracy in the micrometer range [10], with very limited thermal effects to the substrate [11]. The impact of these thermal effects may seem irrelevant for a single-pulse exposure, but it has become a lively field of research for multi-pulse irradiations. That is, the research originates from high-intensity laser light damage of optical components [12]. It has been found that the modification threshold of the materials shows power law drop with increasing number of pulses [13]. This so-called "incubation" involves changes of the material affecting absorption of laser light of the subsequent pulses way ahead of apparent modification of the surface. However, the phenomenon has not yet been explained satisfactorily, although several suggestions have been made in literature, for instance, thermo-plastic deformation in semiconductors [14] and metals [13]. This field of research provides crucial knowledge to avoid damage of optical devices in industrial laser systems, which are exposed to a considerable number of pulses. This knowledge may also contribute to the understanding of the formation of (sub-)wavelength laser-induced periodic surface structures, where initiation and growth of the structures may be influenced by incubation as well [15].

The so-called "zero damage area" or "D^2" method [16] is the commonly accepted method to determine the modification threshold of ultra-short laser pulse irradiation which depends on pulse duration, number of pulses, laser light wavelength, surface finish, and ambient atmosphere. A proper choice of pulse energy, also including the fluence close to the modification threshold, allows an inspection of the first stages of the surface modifications due to laser irradiation, for example, enhancement of absorption on even nanometer-sized surface inhomogeneities. After the laser pulse impingement on these inhomogeneities, one can observe drastic local changes of the surface roughness, due to melting and eruptive expansion of the irradiated matter. All created structures (like spikes, bubbles, sub-micron spheres, etc.) may promote laser light absorption of subsequent pulses. These structures may also significantly contribute to the so-called incubation effect. Copper (Cu) was chosen for these experiments, due to its weak electron–phonon coupling and strong electron thermal conductivity, which will show

* Corresponding author. Tel.: +31 50 363 3407; fax: +31 50 363 4881.
E-mail address: v.ocelik@rug.nl (V. Ocelík).

http://dx.doi.org/10.1016/j.apsusc.2014.02.104
0169-4332/© 2014 Elsevier B.V. All rights reserved.

more evident traces of melting in comparison to transition metals, with strong electron–phonon coupling and weak electron thermal conductivity [17]. Until now, the creation of the surface structures can be explained only to a certain qualitative extent, because computation modeling for process parameters used in our experiments is not available.

Inspection of the surface topography and sub-surface modifications were carried out by scanning electron microscopy (SEM) and transmission electron microscopy (TEM), respectively. Moreover, energy dispersive X-ray spectroscopy (EDS) was employed to obtain information on possible surface chemical interactions. Electron backscattered diffraction (EBSD) was used to study influence of the solidification on crystallography of the surface objects.

The principal aim of the work is to precisely characterize how an ultra-short laser pulse modifies surfaces. The motivation for this research is to show possible surface changes occurring prior to extensive ablation, as well as to fill the lack of data in literature, where mostly only SEM surface inspection is used. Finally, our results may also be used for a comparison with modeling results [11,18].

2. Experimental setup

Polycrystalline copper samples (purity 99.995%), with average crystal grains size of 50 μm, were processed in single-pulse experiments. As a laser source, an Ytterbium-doped YAG (Trumpf TruMicro 5050) was used with laser pulses of 6.7 ps duration and a wavelength of 1030 nm. The linearly polarized laser beam was focused by a 100-mm telecentric F-theta lens (Ronar of Linos, Germany) at normal incidence to the samples surface. The laser beam possesses a Gaussian energy distribution with a $1/e^2$ radius of 13.4 ± 0.2 μm. The average power at the sample surface was measured by a power meter and controlled with the combination of a rotary $\lambda/2$ wave plate and a beam splitting cube. The range of the pulse energies used for the experiments, at 50 kHz pulse repetition rate, was 2.6–92 μJ. The laser spot was scanned over the sample surface by mirrors of a Galvo-scanner (IntelliScan 14 of Scanlab, Germany). Prior to irradiation, the Cu samples were polished, according to metallographic Struers Co. guide [19] with an exception of much lower load applied to the samples. The later limits the sub-surface damage during the first grinding steps and helps to achieve low surface roughness. Grain boundaries were not observed after the final polishing steps, but some minor scratches remained on the surface. The root-mean-square roughness of 3–4 nm was measured on polished samples by confocal microscopy (CM; μSurf Nanofocus optical confocal microscope, 408 nm laser light wavelength). A Philips XL30 SEM, equipped with field emission gun, had a resolution of few nanometers for topography inspection of the samples. Additional EDS spectroscopy and TSL OIM/EBSD detectors on the same microscope allowed chemical and crystallographic analyses, respectively. Cross-sectioning of the surfaces and lamella extraction for TEM observations (JEOL JEM-2010F operating at 200 kV) was done with a focused ion beam system (FIB, Tescan Lyra). An electron beam deposited Pt (EBID-Pt) layer was applied as a surface protection layer during the FIB polishing steps.

3. Results

To determine the minimum threshold fluence level at which modification of the surface occurs as well as to determine laser beam $1/e^2$ radius, the well-known D^2 method was employed [16]. In this experiment, the pulse energy was varied from 15 to 92 μJ and area of the modified surface ($D^2 = 4A/\pi$) was measured by CM after laser irradiation. A fit to semi-log representation of the experimental data yielded a $1/e^2$ beam radius of 13.4 ± 0.2 μm and a threshold

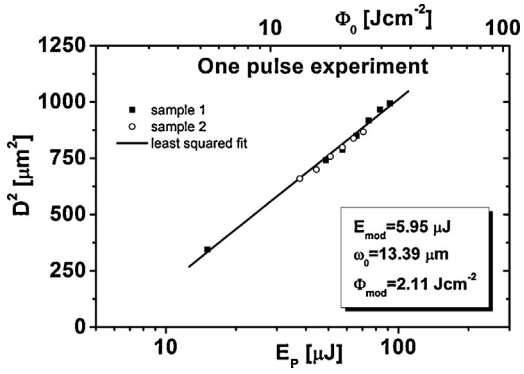

Fig. 1. Squared diameter D^2 of the modified area for single laser pulse exposures on the polished Cu sample by 1030 nm, 6.7 ps laser pulses as function of E_P and Φ_0. The graph is a collection of results on two samples. The fit of the measurements gives $1/e^2$ beam radius (slope of the curve) of 13.4 ± 0.2 μm and a modification threshold of the material (intersection of the extrapolated curve with the horizontal axis) of 2.11 J/cm^2.

fluence of 2.11 J/cm^2 (Fig. 1). The relatively high fluence values of single-pulse modification threshold are associated with the high reflectivity of 97.2% of Cu at a wavelength of 1030 nm [20].

SEM inspection of the irradiated surfaces (Fig. 2(a) and (b)) revealed local surface modifications, at fluence levels even slightly lower than modification threshold obtained via the D^2 method. As seen in Fig. 2(a), it can be caused by laser light absorption on surface topography features such as, for instance, traces of scratches. In this case, however, random modifications did not create a detectable circular modified area. That is why it was not possible to obtain exact diameter for $D^2 = \ln(E_P)$ graph at lower fluence levels. Defect-free surfaces were not obtained. Subsequent decrease in the fluence did not lead to apparent modification of the surface.

As can be observed in Fig. 2, traces of solidification of the molten matter are present on the surface. The specific surface area was significantly enlarged due to objects like thin material membranes (thickness of few tens of nanometers – partially transparent for electrons at 10 kV acceleration voltage), micro-spikes with spherical endings and individual extracted spheres lying freely on the surface. In the case of surface defects with longer lateral dimensions (e.g., the surface scratch in Fig. 2(a), running from the upper left to the lower right in the left part of the picture), the common walls of the neighboring eruptions create a kind of bridging structures with a direction orthogonal to the scratch side walls.

Next, the effect of absorbed laser energy in the copper target and subsequent relaxation of the energy was investigated in detail by cross-sectioning and TEM observations of the irradiated surface (Fig. 3). To obtain a TEM cross-section specimen on a specific location of interest with lateral accuracy of few tens of nanometers, dual-beam FIB system has been applied. Fig. 3 shows that a good alignment of the SEM-SE (SE, secondary electron image), SEM-BSE (BSE, backscattered electron image), and TEM pictures was obtained. It enables a comparison of size and location of the surface thin membranes, spikes with spherical endings, extracted spheres freely lying on the surface, as well as sub-surface defects induced by the laser irradiation. The thickness of the membrane (Fig. 3, the most left-hand side local explosion in TEM picture) is about 30 nm and it seems to be in agreement with the estimation of the value from transparency for electrons in SEM-SE (previous paragraph). The spikes identified from the TEM picture and from Fig. 2(b) show diameters from 40 to 80 nm, depending on the position of measurement on the partially conical objects. Spheres on top of the spikes have various sizes, which do not exceed 140 nm in diameter (Figs. 2, 3 and Fig. 4). Larger spheres lie on the sample surface (Figs. 2, 3 and Fig. 5) and show diameters larger than 200 nm. These spheres have apparently not been produced at the actual

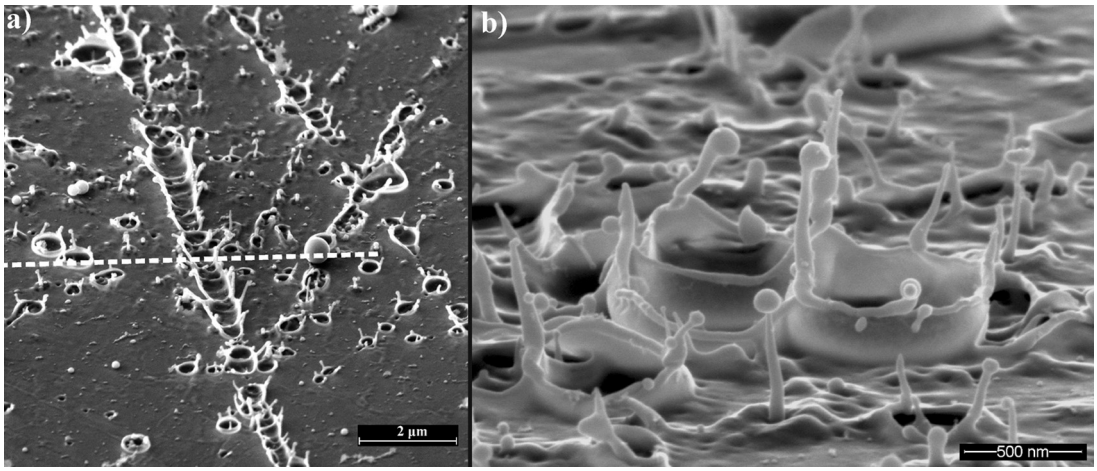

Fig. 2. SEM-SE (SE, secondary electron image) micrographs of the Cu surface treated with a single 6.7 ps laser pulse at a wavelength of 1030 nm and a fluence slightly below 2.11 J/cm^2. These pictures show the center of the modified area at (a) 55° and (b) 75° degree inclination from the surface normal. Surface modification only occurs on local surface defects (particles, scratches). (a) The dashed line indicates the location of cross-sectioning and TEM lamella extraction. (b) Detailed view of the surface shows micro-eruptions.

location of interest (about 300 μm from this location an experiment was performed at fluence significantly higher than the modification threshold and 100 pulses to a single location – not shown here). It suggests that the diameters of these spheres depend on the exposure conditions as is clear from a comparison between diameters of the large spheres with the small ones attached to spike ends. Furthermore, sub-surface modifications at a depth of few tens of nanometers were found. These modifications can be observed as a contrast change at Cu/EBID-Pt interface in Fig. 3 SEM-BSE (also apparent in Fig. 6). This is a result of bombardment and implantation of Ga ions (used in FIB) in this layer of different crystal orientation and density in comparison to the unexposed bulk below.

Next, microscopy inspection of the surface objects was performed in order to investigate the probability of the presence of amorphous material, as well as to study the solidification process of the objects. High-resolution TEM (HRTEM; Figs. 4 and 6) and EBSD (Fig. 7) studies have shown that the structures attached to the surface had a fully crystalline character. No traces of amorphous material were found. The crystal orientation of the spikes, however, does not follow the crystal orientation of the bulk substrate. Contrast changes along the longest spike (Fig. 4(a)) suggest the existence of grains with a different crystal orientation.

High-resolution TEM micrograph (Fig. 4(b)) shows the details of part of grain indicated by the white frame and arrow in Fig. 4(a). An angle of 24.4° was measured between the (111) planes of the spike ending and the bulk substrate below, as indicated in Fig. 4(b). The direction of the $(111)_{\text{Cu matrix}}$ is depicted. The head of the spike is bent with respect to the axis of body of the spike. This angle is about 60° clockwise in the picture plane, however, the crystal (111) plane is 24.4° inclined. EBSD measurements (see the pole figure in Fig. 7) showed strong and random scatter of crystal orientations in

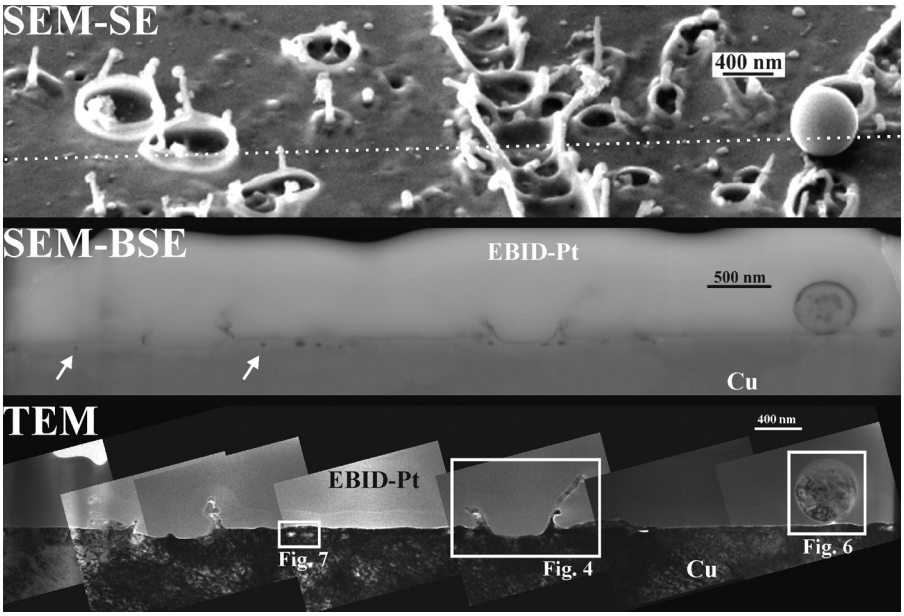

Fig. 3. Detailed microscopy inspection of the Cu surface irradiated by a single ultra-short laser pulse at fluence just below the modification threshold. The SEM-SE micrograph (top) is a close-up of that in Fig. 2(a). The dotted line indicates the approximate location of the FIB cross-sectioning and subsequent TEM lamella extraction. The SEM-BSE (center) is a cross-sectional view of the Cu surface covered with EBID-Pt protective layer during FIB lamella preparation. In this micrograph, the white arrows indicate sub-surface defects. The TEM (lower) picture shows the same cross-section created by transmitted electrons through the lamella with a thickness of about 75 nm.

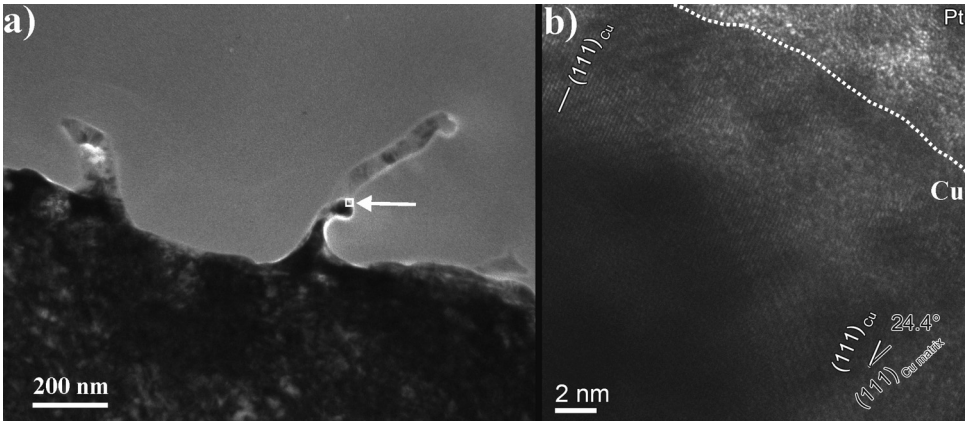

Fig. 4. (a) High-magnification TEM image of a micro-eruption on the laser-machined Cu surface. Splashes of material form spikes with a diameter of a few tens of nanometers. Contrast changes in the largest spike (right spike in (a)) visible during specimen tilting in TEM suggest a polycrystalline character of the object. (b) High-resolution TEM micrograph shows a detail of the location indicated by the white frame and arrow in (a). An angle of 24.4° is measured between the (111) planes of the spike ending and the bulk. The dotted line decorates the interface between Cu and EBID-Pt.

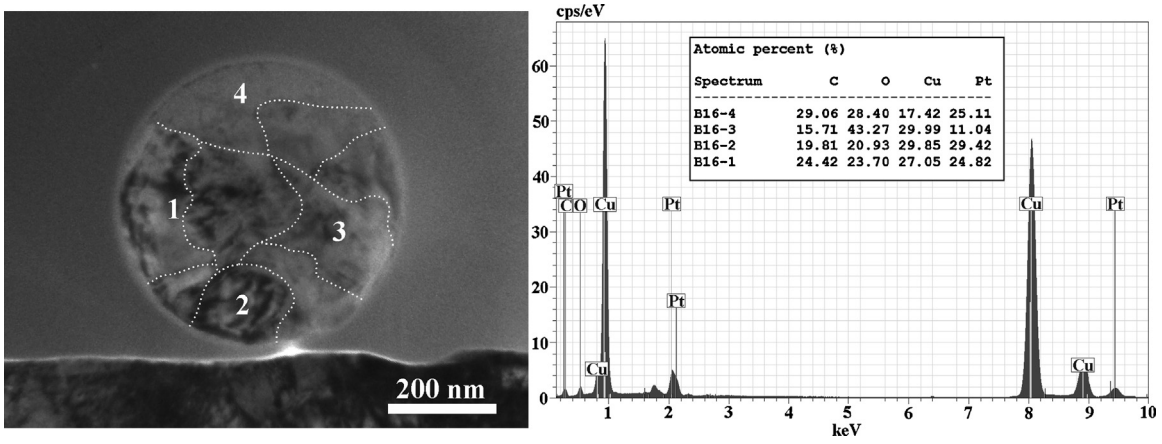

Fig. 5. EDS measurements of the sphere from Fig. 3 (TEM). The left TEM micrograph shows crystal boundaries according to HRTEM inspection, which are highlighted with dotted lines. EDS measurements were conducted in four locations and the corresponding elements content is shown in the graph on the right. The amount of Pt and C is attributed to contamination of the sphere cross-section surface by EBID-Pt material re-deposited during polishing steps. The amount of oxygen is attributed to copper oxides created during solidification.

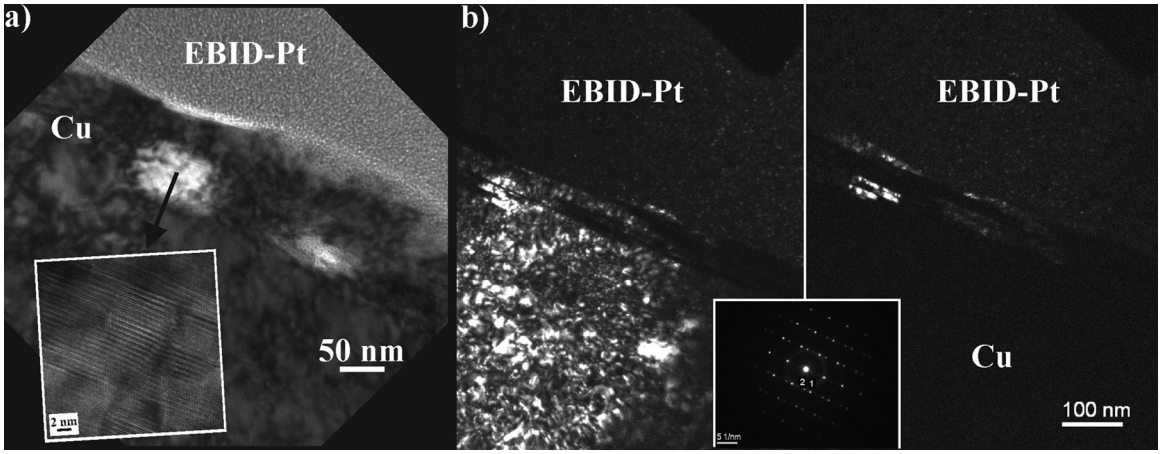

Fig. 6. TEM images of sub-surface changes induced by a single ultra-short laser pulse. (a) High-magnification detail of the location highlighted in Fig. 3 (TEM). There are two sub-surface defects at a depth of approximately 50 nm. HRTEM inset of (a) image shows the details of the material twinning. The bright right-hand side object is a sub-surface void filled with EBID-Pt deposit. The two TEM pictures in (b) represent Cu–EBID(Pt) interface and the sub-surface twins separated by dark field imaging. The inset in (b) shows an electron diffraction pattern from this area.

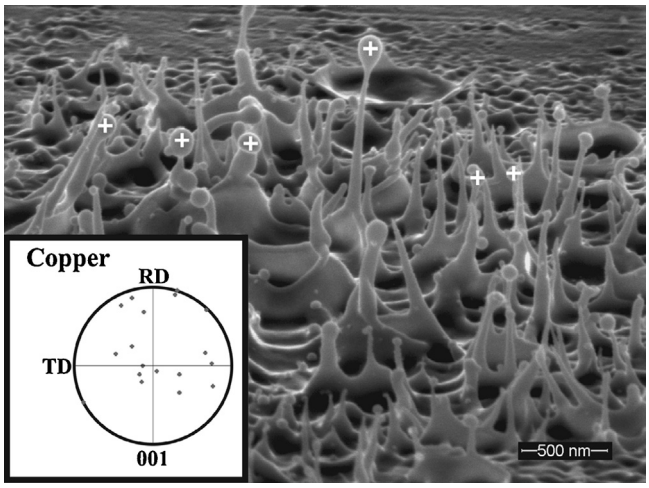

Fig. 7. (a) SEM-SE micrograph of the Cu surface after a single-pulse exposure. The fluence of 3.55 J/cm^2 was slightly higher than the single-pulse modification threshold. Insert: (001) pole figure of EBSD measurement showing random crystal orientation of the head of the spikes (indicated by white crosses, RD, rolling and TD, transversal directions).

the head of the spikes. In this case, the spikes are taller than those in Figs. 2–4, due to irradiation conditions slightly over the one-pulse modification threshold fluence.

The main part of the larger spheres is crystalline, as is suggested by the dotted lines along crystal boundaries and contrast differences in TEM micrograph of Fig. 5. However, when compared to Fig. 3 SEM-BSE, one can observe dark areas, which are almost circular, within the sphere. These areas are typical for all spheres of this size and these areas point at contamination during the solidification process. A supplement EDS measurement has shown a remarkable amount of oxygen within the sphere, as well as carbon and platinum. The amount of oxygen at the location, indicated by number 3 in Fig. 5, is higher than the average value. This is interpreted as a tendency of Cu oxides to agglomerate in particular locations during solidification.

Laser-induced sub-surface structures were observed in cross-section, both by SEM (Fig. 3, SEM-BSE) and by TEM (Fig. 6) imaging including structures like isolated defects, defects in proximity of surface micro-eruptions, and continuous sub-surface material twinning.

Two local defects, indicated by white arrows in Fig. 3 SEM-BSE, show diameters of about 40 nm. The shortest distance of these defects to the neighboring micro-eruptions is at least 250 nm. These defects show a small volume and are almost spherical in shape, as they appear and disappear (comparison SEM-BSE to TEM) during the last few very gentle polishing steps. It suggests that the defects are sub-surface voids. Moreover, detailed inspection of the TEM lamella shows cross-sectional view of two additional surface features: the presence of material twinning, as well as cross-section of a surface micro-eruption (Fig. 6, highlighted in Fig. 3 TEM). The micro-eruption cross-section in Fig. 6(a) (right-hand side, brighter spot) is filled with Pt nano-grains enclosed in carbonaceous matrix (EBID-Pt), which implies that this location was exposed to the surface prior to the EBID-Pt deposition. The presence of the surface material twinning is clear from the inset of Fig. 6 (a). Alternation of the twins occurs with a periodicity of few atomic planes. This part of the surface was also inspected at a lower magnification by electron diffraction (Fig. 6(b) inset). Dark field imaging was helpful to separate two crystal orientations (Fig. 6(b) left and right), observable in the electron diffraction pattern. The separated crystal orientations reveal that the sub-surface twinning is present to a depth of 50–60 nm.

4. Discussion

Theoretical explanations of ultra-short laser pulses interaction with metal surfaces has been attempted since the 1970s [21]. The laser–material interaction is usually described as a one-dimensional version of two coupled nonlinear differential equations, which track the temporal temperature evolution of the free electron gas and phonons of the material and is known as the two-temperature model (TTM). The maximum temperature of the target surface depends on the laser parameters (wavelength, pulse duration) and the material properties (reflectivity, light penetration depth, electron and lattice heat capacity, electron thermal conductivity, and electron–phonon coupling factor). Recently, the predictive power of the TTM model has been strengthened by the incorporation of molecular dynamics (MD) [18]. It allows substitution of TTM equation for temperature of the phonons by MD in a surface layer, where the most significant processes are expected to occur, near or at higher temperatures than the material melting point. Published results on various materials [11,18,22] obtained by this advanced TTM-MD model provide insights into the phenomena involved in the relaxation of the absorbed laser pulse energy. However, the origin of micro-eruptions on the Cu target surface found in our experiments can be explained only to a certain qualitative extent due to two reasons. First, there is a lack of computational modeling in literature for our processing conditions (pulse duration and laser wavelength). Secondly, articles published on this topic concentrate on ideal conditions, that is, defect-free atomically flat initial surfaces. The first reason seems to be marginal when absorbed fluence (Φ_a) in the material instead of nominal (Φ) is taken as a base for comparison of our results to the results of Schäfer et al. [18]. It should be noted that the equation $\Phi_a = (1-R)\Phi$, where R is the reflection coefficient of the material, brings us to comparable values of Φ_a. When the ablation threshold fluence 0.17 J/cm^2 (nominal fluence, [18]) and 2.11 J/cm^2 (nominal fluence in this work) are multiplied by corresponding reflection coefficients in UV ($1-R = 0.4$, [18]) and IR spectra ($1-R = 0.03$, [20]), it yields Φ_a equal to 0.068 and 0.063 J/cm^2, respectively. Hence, the absorption fluence levels are comparable, difference in pulse duration (0.5 ps in Ref. [18] and 6.7 ps in our experiments) should not markedly influence the physics of the laser energy relaxation, because the time interval for relaxation of the laser-induced thermo-elastic stresses in Cu is more than two times larger (19 ps [18]) than the pulse duration. In a qualitative way, the surface imperfections can be understood as local absorption amplifiers, that is, they just result in local increase in the surface temperatures.

Theoretical simulations of laser–matter interaction [11,18,22,23] suggest three characteristic regimes of energy relaxation with increasing laser pulse fluence. That is, melting, photo-mechanical spallation, and phase explosion. Only spallation and phase explosion are processes responsible for extensive material transport and material removal from the irradiated surface. Spallation ejects molten material from the surface due to laser-induced tensile stresses [11]. The ablation behavior changes abruptly when the irradiated matter reaches temperatures close to the critical point in phase diagram which turns it into a mixture of liquid droplets and gas atoms. The simulation presented in Ref. [11] shows that the difference between spallation and phase explosion thresholds is very small. Comparison of the theoretical models with the local explosions observed in our SEM micrographs (Fig. 2) indicates a mixture of both phenomena. Predominance of one of them may strongly depend on shape and size of the surface defects (i.e., absorption enhancement), as well as on the nominal fluence. The absorbed laser fluence and intensity consequently determine molten material properties (viscosity, density, and surface tension are temperature dependent [24]) and expansion speed of the micro-eruptions. Taking into account typical

expansion speeds of the irradiated matter in spallation regime to be at 50–400 m/s [11,18] and the diameter of the micro-eruptions in our experiments around 750 nm (Fig. 2(b)) leads to an expansion time (i.e., solidification) between 1.9 and 15 ns. A rough estimate of cooling rates (latent heat not taken into account) then gives values larger than 10^{11} K/s for initial temperatures exceeding the melting point of Cu 1358 K (calculation not shown here for the sake of concision). It has been shown in our TEM inspection that even these extreme fast cooling rates do not create amorphous phase in pure copper. It is worth mentioning that standard methods for the preparation of metallic glasses, for example, splat cooling [25] introduced in 1960s, induce amorphous phase at cooling rates as low as 10^6 K/s, however, the techniques succeeded only in the case of multi-compositional alloy systems.

4.1. Spikes with spherical ends

Figs. 2–4 and 7 show that the origin of spikes is related to expansion of irradiated matter. Energy absorbed in the surface defects (scratches, particles etc.) relaxes via some kind of micro-eruptions, due to spallation, phase explosion, or potentially both acting simultaneously. Animated sequences in Refs. [18,26] indicate the role of inertia, viscous, and capillary forces in modification of the surface topography. At moderate fluences, molten material creates thin membranes as a consequence of expansion of neighboring voids. At fluence levels just above the ablation threshold (animation for 15 ps pulse in Ref. [26]) a continuous liquid layer propagating from the surface is visible. The creation of a cupola or a bubble appears, like those seen in Figs. 2(a) and (b). After creation of a hole in the thin membranes, the vapor pressure in the bubbles tends to equalize with the ambient atmosphere. The induced flow of material bends the rim of the hole outwards as can be seen in Fig. 2(b) and Ref. [24]. Viscous and capillary forces in the thin membranes cause its continuous contraction. Finally, membrane collapses into spikes as well as spheres extracted or detaching from the spikes.

After solidification, the crystal orientation of the spikes differs from the bulk. This has been shown by contrast difference in the long spike in Fig. 4 and the crystal (111) plane mismatch of the small spike head in the same picture. Measurement of crystal orientation scatter in Fig. 7 has proven this.

4.2. Extracted spheres

For extracted spheres, heat radiation will be the predominant process for energy dissipation, and as a result, spheres in Fig. 2 are solidified before impact on the surface. Arguments supporting this statement are: the spherical shape, almost no contact with sample surface and lower estimate of their stay in the ambient atmosphere in the microsecond range (300 μm distance mentioned in results section, 50 m/s lower estimate of expansion speed, direct trajectory, and neglected resistance of the ambient gas). Upper bound of the time required for sphere solidification could be roughly derived from Stefan–Boltzmann law. Emissivity of 0.15 was used to calculate the cooling of Cu ball with diameter of 500 nm (the size shown in Fig. 5). It is estimated to dissipate the heat between boiling and melting temperature in 2 ms with an average cooling rate of 7.5×10^5 K/s. During this time, the heat content, three times higher than heat of fusion, is released. It is reasonable to expect complete solidification of the ball in time shorter than 3 ms. Oxidation in liquid state may change solidification conditions. The cooling time is four times shorter (0.5 ms, 1.3×10^6 K/s) for CuO and 6.7 times shorter for Cu_2O (0.3 ms, 1.9×10^6 K/s) balls with the same diameters. Heat content is approximately equal to heat of fusion for CuO and 50% of heat of fusion for Cu_2O. When heat of formation (oxidation), which is close to heat of fusion, is taken into account, the solidification time is not expected to exceed 3 ms. This estimated number 3 ms can be further decreased by the fact that starting temperature of the cooling is highly likely lower than boiling temperature.

The relatively longer stay of spheres in ambient air, prior to solidification, can explain the measured high content of oxygen in the sphere (EDS in Fig. 5). Impurities in the form of oxides tend to agglomerate during solidification. It can be recognized as a contrast difference in Fig. 3 SEM-BSE, due to interaction of Ga ions (FIB) with material of different density (ρ(Cu) = 8.96 g cm^{-3}, ρ(CuO) = 6.32 g cm^{-3}, or $\rho(Cu_2O)$ = 6.0 g cm^{-3} at room temperature). The oxygen content cannot have another origin than oxidation of Cu before and during solidification, due to the following reasons. The high oxygen level is only found in these spheres and the untreated surface has no detectable oxygen. It is important to mention that the samples were laser processed right after polishing and they were kept under vacuum after processing. A possible source of the contamination of the sphere cross-section, during polishing steps (EBID-Pt protective layer), is oxygen free $(CH_3)_3(CH_3C_5H_4)Pt$. The last argument explains the quite high content of Pt and C in the EDS measurements.

4.3. Sub-surface defects

Creation of sub-surface voids has been recently reported in Ref. [11] and their possible disappearance is shown in Ref. [26] for 15 ps laser pulses. The strength of tensile stress induced in a laser irradiated layers depends on absorbed fluence of the incident laser pulse, if conditions of stress confinement are fulfilled. It means that the pulse duration is shorter than the time needed to reach mechanical equilibrium [18]. The conditions for the initiation of voids should be fulfilled for irradiation of almost all materials at sub-10 ps pulse durations [11,18,22,23]. At fluence levels higher than modification threshold nucleation, expansion and subsequent coalescence of sub-surface voids occur. It leads to the repulsion of larger amounts of molten material from the surface (spallation), which leaves behind contracting membranes and spikes [26]. At fluences lower than modification threshold, however, magnitude of the tensile stress seems to be sufficient for nucleation of voids, but not for their subsequent expansion. Simulations in Ref. [26] with 15 ps laser pulses and a fluence below the modification threshold showed that voids can also disappear within a time range of a few hundred of picoseconds after the laser pulse impingement. Here, one can propose the possibility of voids “freezing” when the solidification is faster than the contraction of the voids (Fig. 3 SEM-BSE).

Sub-surface twinning in Fig. 6(a) inset or Fig. 6(b) is a result of strains induced in the material. Dark field imaging showed the presence of the twins only at depths of about 50–60 nm. This depth is estimated to be comparable to heat affected zone of the material due to heat transfer at lower fluence levels electron heat diffusion length 65 nm [10]). The heat transfer is a source of plastic strain in the material according to Ref. [13]. When the amplitude of the thermal stress induced by the laser pulse exceeds the plastic yield point, it subsequently leads to localized plastic deformation and twinning.

Two groups of surface and sub-surface modifications are induced by the ultra-short laser pulse. They are either created at already present surface inhomogeneities due to polishing and insufficient cleaning, or they belong to thermal sub-surface modifications under reasonably flat surfaces. Irrespective of their origin, both occur at fluence levels lower than the single-pulse modification threshold and they markedly change optical properties of the material for subsequent laser pulses. These imperfections, in combination with metallic absorption of light, can contribute to explanation of the “non-physical” zero modification threshold

fluence for infinite number of pulses arising from Jee's empirical equation for incubation in metals [13].

5. Conclusion

Surface modifications induced on mirror-polished Cu surfaces under irradiation of single laser pulses with 6.7 ps and 1030 nm were studied. The so-called D^2 method was employed for obtaining the single-pulse modification threshold. Attention has been directed to the investigation of the surface modifications created at a fluence level close to the threshold. Thermally induced topography and sub-surface changes were analyzed using electron microscopy techniques in order to improve the understanding of the origin of the laser-induced modifications. Conclusions of the investigation are as follows:

- The single-pulse modification threshold of the material and the $1/e^2$ beam radius obtained via D^2 method are 2.11 J/cm^2 and 13.4 ± 0.2 μm, respectively.
- Fluence level below the single-pulse modification threshold is high enough for local changes to the surface. This modification is caused by enhanced laser absorption by surface imperfections even of nanometer sizes.
- Local surface micro-eruptions create: membranes with thickness under 50 nm, spikes with a typical length in the micron range and sub-micron diameters, spheres extracted from spike endings with (usually) sub-micron diameter, which depends on process conditions.
- The estimated high cooling rates, induced by ultra-short laser pulses, are larger than 10^{11} K/s and they do not lead to amorphous phase creation during the solidification process.

Acknowledgement

This research was carried out under project number M61.3.08300 in the framework of the Research Program of the Materials innovation institute M2i (www.m2i.nl).

References

[1] Q.-Z. Zhao, S. Malzer, L.-J. Wang, Self-organized tungsten nanospikes grown on subwavelength ripples induced by femtosecond laser pulses, Opt. Express. 15 (2007) 15741.
[2] J.P. Colombier, F. Garrelie, N. Faure, S. Reynaud, M. Bounhalli, E. Audouard, et al., Effects of electron-phonon coupling and electron diffusion on ripples growth on ultrafast-laser-irradiated metals, J. Appl. Phys. 111 (2012), 024902-024902-6.
[3] J. Bonse, J. Krüger, S. Höhm, A. Rosenfeld, Femtosecond laser-induced periodic surface structures, J. Laser Appl. 24 (2012), 042006-042006-7.
[4] A. Borowiec, H.K. Haugen, Subwavelength ripple formation on the surfaces of compound semiconductors irradiated with femtosecond laser pulses, Appl. Phys. Lett. 82 (2003) 4462–4464.
[5] T.H.R. Crawford, H.K. Haugen, Sub-wavelength surface structures on silicon irradiated by femtosecond laser pulses at 1300 and 2100 nm wavelengths, Appl. Surf. Sci. 253 (2007) 4970–4977.
[6] D. Ashkenasi, R. Stoian, A. Rosenfeld, Single and multiple ultrashort laser pulse ablation threshold of Al2O3 (corundum) at different etch phases, Appl. Surf. Sci. 154–155 (154) (2000) 40–50.
[7] M. Shinoda, R.R. Gattass, E. Mazur, Femtosecond laser-induced formation of nanometer-width grooves on synthetic single-crystal diamond surfaces, J. Appl. Phys. 105 (2009), 053102-053102-4.
[8] Y. Shimotsuma, P.G. Kazansky, J. Qiu, K. Hirao, Self-organized nanogratings in glass irradiated by ultrashort light pulses, Phys. Rev. Lett. 91 (2003) 247405.
[9] V.R. Bhardwaj, E. Simova, P.P. Rajeev, C. Hnatovsky, R.S. Taylor, D.M. Rayner, et al., Optically produced arrays of planar nanostructures inside fused silica, Phys. Rev. Lett. 96 (2006) 057404.
[10] S. Nolte, C. Momma, H. Jacobs, A. Tünnermann, B.N. Chichkov, B. Wellegehausen, et al., Ablation of metals by ultrashort laser pulses, J. Opt. Soc. Am. B. 14 (1997) 2716–2722.
[11] L.V. Zhigilei, Z. Lin, D.S. Ivanov, Atomistic modeling of short pulse laser ablation of metals: connections between melting, spallation, and phase explosion, J. Phys. Chem. C 113 (2009) 11892–11906.
[12] C.S. Lee, N. Koumvakalis, M. Bass, Spot-size dependence of laser-induced damage to diamond-turned Cu mirrors, Appl. Phys. Lett. 41 (1982) 625–627.
[13] Y. Jee, M.F. Becker, R.M. Walser, Laser-induced damage on single-crystal metal surfaces, J. Opt. Soc. Am. B. 5 (1988) 648–659.
[14] G.D. Tsibidis, E. Stratakis, K.E. Aifantis, Thermoplastic deformation of silicon surfaces induced by ultrashort pulsed lasers in submelting conditions, J. Appl. Phys. 111 (2012), 053502-053502-12.
[15] J. Eichstädt, G.R.B.E. Römer, A.J. Huis in 't Veld, Determination of irradiation parameters for laser-induced periodic surface structures, Appl. Surf. Sci. 264 (2013) 79–87.
[16] J.M. Liu, Simple technique for measurements of pulsed Gaussian-beam spot sizes, Opt. Lett. 7 (1982) 196–198.
[17] Z. Lin, L.V. Zhigilei, V. Celli, Electron-phonon coupling and electron heat capacity of metals under conditions of strong electron-phonon nonequilibrium, Phys. Rev. B 77 (2008) 075133.
[18] C. Schäfer, H.M. Urbassek, L.V. Zhigilei, Metal ablation by picosecond laser pulses: A hybrid simulation, Phys. Rev. B 66 (2002) 115404.
[19] http://www.struers.com.
[20] http://refractiveindex.info/.
[21] S.I. Anisimov, B.L. Kapeliovich, T.L. Perel'man, Electron emission from metal surface exposed to ultrashort laser pulses, J. Exp. Theor. Phys. 39 (1974) 375–377.
[22] http://www.faculty.virginia.edu/CompMat/Resources.html.
[23] L.J. Lewis, D. Perez, Laser ablation with short and ultrashort laser pulses: Basic mechanisms from molecular-dynamics simulations, Appl. Surf. Sci. 255 (2009) 5101–5106.
[24] J.C.d.R. Bird, Daughter bubble cascades produced by folding of ruptured thin films, Nature 465 (2010) 759–762.
[25] W. Klement, R.H. Willens, P. Duwez, Non-crystalline structure in solidified gold–silicon alloys, Nature 187 (1960) 869–870.
[26] http://people.virginia.edu/~lz2n/ablation/animations/.